PLANETARY SCIENCE

Zircon trace element evidence for early hydrothermal activity on Mars

Jack Gillespie[1,2]*, Aaron J. Cavosie[2,3], Denis Fougerouse[2,4], Cristiana L. Ciobanu[5], William D. A. Rickard[2,4], David W. Saxey[2,4], Gretchen K. Benedix[3], Phil A. Bland[3]

Finding direct evidence for hydrous fluids on early Mars is of interest for understanding the origin of water on rocky planets, surface processes, and conditions essential for habitability, but it is challenging to obtain from martian meteorites. Micro- to nanoscale microscopy of a unique impact-shocked zircon from the regolith breccia meteorite NWA7034 reveals textural and chemical indicators of hydrothermal conditions on Mars during crystallization 4.45 billion years ago. Element distribution maps show sharp alternating zoning defined by marked enrichments of non-formula elements, such as Fe, Al, and Na, and ubiquitous nanoscale magnetite inclusions. The zoning and inclusions are similar to those reported in terrestrial zircon crystallizing in the presence of aqueous fluid and are here interpreted as primary features recording zircon growth from exsolved hydrous fluids at ~4.45 billion years. The unique record of crustal processes preserved in this grain survived early impact bombardment and provides previously unidentified petrological evidence for a wet pre-Noachian martian crust.

INTRODUCTION

Hydrothermal systems are considered critical for the development of life, and so understanding the origin, distribution, and duration of such environments in the geological record of Mars is of primary interest (*1*). Spacecraft data have documented fluvial landforms and widespread occurrences of phyllosilicates in Noachian crust that record the action of surface water on Mars before ~3.8 billion years (Gyr) ago (*2*–*4*). Hydrothermal systems have also been implicated in the generation of strong remnant magnetization of the martian crust, which preserves a record of the existence of a geodynamo in the early part of martian history (*5*). A better understanding of the timing of hydrothermal activity is critical, therefore, not only for a better understanding of surface hydrology but also for the deep structure of Mars.

The group of martian meteorites comprising Northwest Africa 7034 (NWA7034) and 18 paired stones (*6*) are polymict regolith breccias and represent the only available samples of the surface of Mars. These meteorites are useful for studying water on early Mars due to several important properties: They contain a high abundance of very ancient [~4.4 billion years (Ga)] material compared to other classes of martian meteorites, they are unusually water rich, and they are highly magnetized (*7*, *8*). They collectively represent a unique archive to understand the timing and origin of hydrothermal activity on Mars and the connection with a highly magnetized Noachian crust (*9*).

This study focusses on an impact-shocked zircon grain previously identified in a chip of the NWA7034 polymict regolith breccia (*10*). This grain contains {112} deformation twins and is now the only reported zircon from Mars in which diagnostic evidence for shock deformation has been documented (*11*). The deformation twins record high-pressure shock conditions (>20 GPa) (*12*, *13*) as the result of a meteorite impact experienced by the grain during its history. The lack of high-pressure shock indicators in other zircon grains (*11*) and other minerals in the breccia sample (*14*, *15*) indicates that the impact event recorded by this zircon predates formation of the regolith breccia and, thus, is unrelated to its ejection from the surface of Mars. The studied grain is an angular fragment broken from a larger zircon; previous U-Pb dating by ion microprobe of this zircon produced a concordant age of 4452.7 ± 17.4 million years (Ma) (*10*). This age places crystallization of the zircon in the midst of the oldest population of zircons from Mars (4.48 to 4.43 Ga) (*16*, *17*).

Here, we apply a suite of micro- to nanoscale analytical techniques including scanning electron microscopy (SEM), time-of-flight–secondary ion mass spectrometry (ToF-SIMS), transmission electron microscopy (TEM), and atom probe tomography (APT) to investigate the geochemical and textural distribution of trace elements in this unique grain. In particular, we focus on non-formula elements that are not typically incorporated in zircon during magmatic crystallization. We then explore the implications of trace element distribution in this zircon for understanding the early development of Mars.

RESULTS

Growth zoning defined by non-formula elements

Cathodoluminescence (CL) imaging reveals that the zircon contains regular growth zones that correspond to {111} and {100} crystal faces (Fig. 1A). Electron backscatter diffraction analysis shows that the {112} deformation twins (Fig. 1B) (*10*) crosscut the growth zones. Ion imaging by ToF-SIMS probed the polished surface of the grain with a ~100-nm lateral resolution, in regions away from cracks and the grain margin (Fig. 1A). The ion images show that the growth zones are defined by micrometer-wide (1 to 10 μm) bands of non-formula elements including Fe, Al, and Na in parallel layers of alternating intensity that are coherent with banding visible in CL (Fig. 1). Heterogeneities in the sub-micrometer-scale element distribution within these bands are readily apparent at length scales an order of magnitude smaller than the growth zones, particularly for Fe (Fig. 1C). A

[1]Institute of Earth Sciences, Faculty of Geosciences and Environment, University of Lausanne, Lausanne CH-1015, Switzerland. [2]School of Earth and Planetary Sciences, Curtin University, Perth, Bentley WA 6845, Australia. [3]Space Science and Technology Centre, School of Earth and Planetary Sciences, Curtin University, Perth Bentley WA 6845, Australia. [4]Geoscience Atom Probe Facility, John de Laeter Centre, Curtin University, Perth, Bentley WA 6845, Australia. [5]School of Chemical Engineering, The University of Adelaide, Adelaide, SA 5005, Australia.
*Corresponding author. Email: jack.gillespie@unil.ch

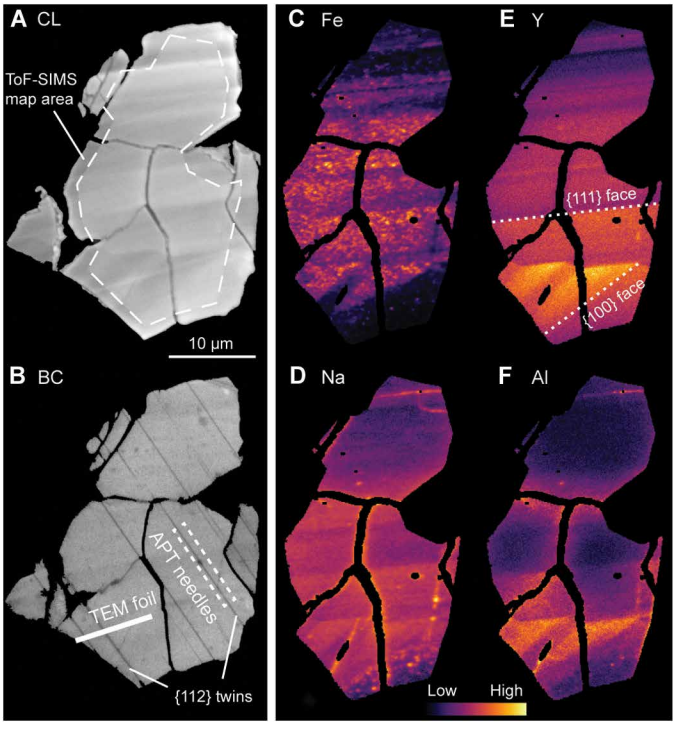

Fig. 1. Micrographs of the shocked martian zircon grain showing key features. (**A**) Cathodoluminescence (CL) image with visible banding in zircon, showing the area analyzed by ToF-SIMS. (**B**) Band contrast (BC) image from electron backscatter diffraction analysis showing planar features including {112} shock twins, in addition to the locations of TEM foil and APT needles. (**C** to **F**) ToF-SIMS maps showing relative Fe, Y, Na, and Al abundance variations.

heterogeneous elemental distribution is also apparent for Na, although to a lesser degree (Fig. 1D), whereas other elements (Y and Al) appear to be homogeneously distributed within growth zones (Fig. 1, E and F). No variation in the distribution of these trace elements associated with the shock twins was detected at the resolution of ToF-SIMS analysis.

Deformation of magnetite inclusions by shock twins

To further resolve the heterogeneous nature of Fe distribution at sub-micrometer scale, we extracted a thin foil from the zircon for analysis by energy-dispersive x-ray spectroscopy using scanning TEM (EDS-STEM) (Figs. 1B and 2A). Within the foil, the {112} shock twins dip at ~60°. Ubiquitous 10- to 100-nm-sized magnetite inclusions are visible in high-angle annular dark-field (HAADF) images (Fig. 2, B to D). Some magnetite inclusions in the vicinity of the shock twin planes exhibit conspicuous lattice deformation that is not present in magnetite inclusions elsewhere (Fig. 2B). The termination of a zircon {112} twin plane at the margin of a magnetite inclusion (Fig. 2D) provides a critical crosscutting relationship, showing that {112} twin formation postdated formation of the magnetite inclusions. All studied magnetite inclusions are located within well-ordered domains of zircon that preserve no indication of radiation damage at a TEM scale. The concentrations of minor elements in the TEM foil were measured by EDS-STEM and yield compositions of ~0.5 atomic % (at %) Y, 1.0 to 1.3 at % Fe, and 0.3 to 0.8 at % Al (table S1). High-resolution EDS-STEM analysis further shows the highly crystalline nature of the zircon and also found conspicuous nanometer-scale enrichments in Fe along the {112} twin planes (Fig. 2, E and F).

Atom-scale distribution of Fe-Al-Y

The distribution of Fe, Al, and Y at an atom scale was investigated by APT analyses of zircon specimens extracted from one of the shock twins (see location in Fig. 1B). Clusters defined by a 0.34 at % Y isoconcentration surface have an average diameter of 4 nm and are enriched in Fe, Al, and Y (Fig. 3, A to C), with compositions of 0.0 to 2.1 at % Fe, 0.0 to 1.4 at % Al, and 0.4 to 3.7 at % Y (Fig. 3D and table S2). The Fe and Y concentrations in the clusters display an inverse relationship, with values varying continuously across the compositional ranges (Fig. 3D); Al contents had a weak inverse relationship to Y contents. The size of the nanoscale Fe-bearing clusters observed by APT is distinctly smaller than the magnetite inclusions observed in TEM images (Fig. 3C). The larger magnetite inclusions are clearly distinguishable by chemical composition from the smaller Fe-rich clusters within the zircon.

DISCUSSION

Hydrothermal origin of growth zoning

Growth zones in the martian zircon are defined by high concentrations of Fe, Al, and Na (Fig. 1), which are not typical elements that partition into zircon during magmatic crystallization (*18*). The lack of alteration features makes it difficult to envisage wholesale incorporation of trace elements and inclusions at some later geologic time without also disturbing and/or age resetting the U-Pb isotopic system of the zircon (*19*). The regular banding defined by non-formula elements observed in this zircon shares some similarities to growth zones defined by Fe, Ca, and Cl observed in zircons from granites in the Mesoproterozoic Olympic Province of South Australia, which are, likewise, interpreted to have been produced by fluids exsolved during magmatic crystallization (*20*). We thus argue that the martian zircon grew during a high-temperature hydrothermal event at 4.45 Ga (the concordant U-Pb age obtained for the zircon), involving contemporaneous crystallization of both zircon and magnetite from an oxidizing hydrous fluid. This is consistent with other evidence for the exsolution of oxidizing fluids during igneous crystallization from studies of lithic clasts within the NWA7034 regolith breccia (*15*).

Significance of nanoscale magnetite inclusions

Textural characteristics and petrogenesis of magnetite inclusions within terrestrial zircon have been investigated previously because of their significance as a carrier phase for ancient magnetic paleointensity records (*21*–*24*). Direct observations of magnetite inclusions in igneous zircon by SEM and TEM find that they most commonly occur in textural features indicative of alteration or damage, such as cracks, pores, and in metamict (radiation damaged) zones, and are, therefore, typically considered to represent a secondary alteration mineral rather than a primary magmatic mineral (*22*, *23*, *25*). In contrast, the magnetite inclusions described here are encapsulated within pristine zircon that records no evidence of radiation damage, lattice recovery, or fluid alteration (Fig. 2). The lack of observed radiation damage at the TEM scale is consistent with low U [28 to 46 parts per million (ppm)] and Th (23 to 39 ppm) concentrations (*10*), which limit the maximum accumulated alpha-recoil damage since crystallization to a calculated dose of 4.8×10^{17} to 8.0×10^{17}

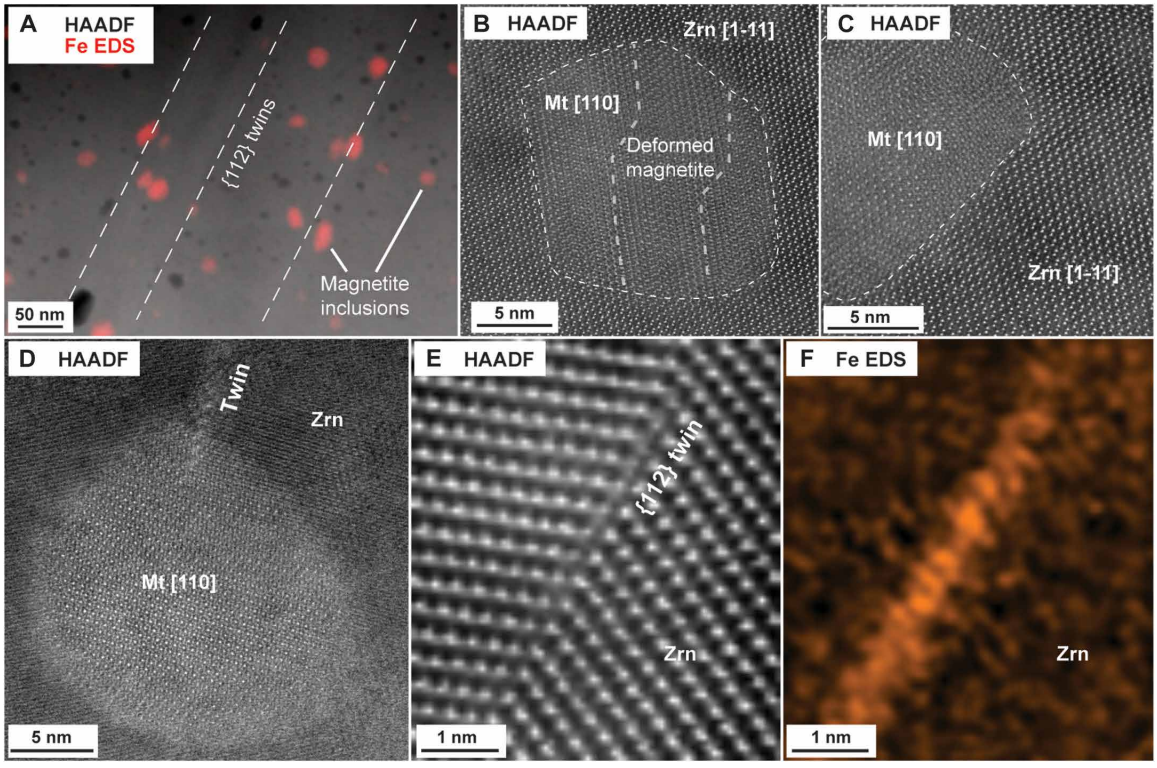

Fig. 2. TEM images of nanoinclusions and twin planes within the zircon. (**A**) Distribution of magnetite inclusions within the zircon relative to {112} twins, (**B** and **C**) magnetite inclusions within zircon, (**D**) termination of a zircon {112} twin at magnetite inclusion, and (**E** and **F**) {112} deformation twin in zircon, with elevated Fe counts along the twin plane.

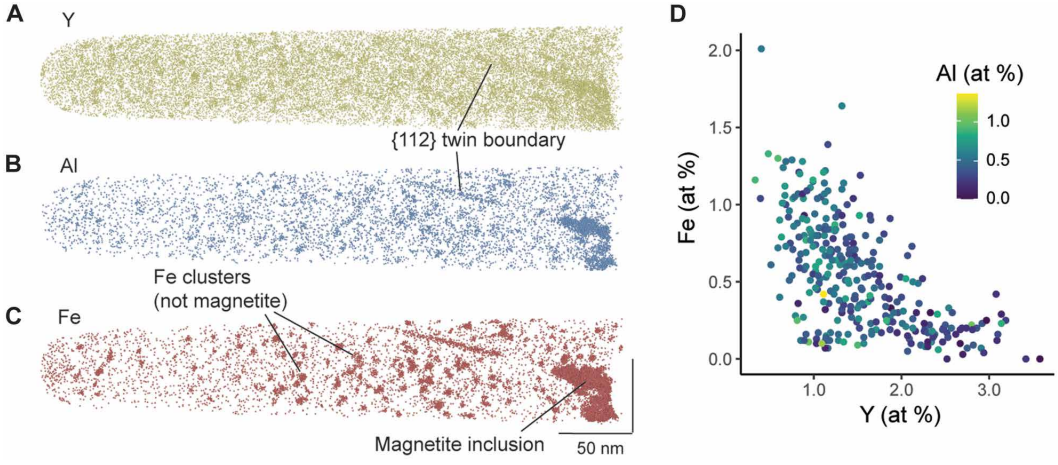

Fig. 3. APT reconstruction showing non-formula element distributions in the shocked martian zircon. (**A** to **C**) Y, Al, and Fe clusters, and (**D**) composition of trace element clusters within the zircon showing concentrations of Y, Fe, and Al in units of atomic %.

α/g, a value far below the first percolation threshold (~2×10^{18} α/g) (*26*). We thus interpret that the magnetite inclusions are primary features that originated by co-crystallization of magnetite and zircon at 4.45 Ga.

Trace element cluster formation by meteorite impact

Nanoscale trace element clustering in zircon resolved by APT has been shown to reveal a variety of cryptic processes related to igneous, metamorphic, and alteration events that cannot be detected by other means (*24*, *27*, *28*). Trace element clusters in ancient terrestrial zircon have been interpreted to form by thermally activated diffusion over several million years at high temperatures (*27*, *29*) and also in response to short-duration shock metamorphism during meteorite impact (*28*, *30*).

Numerous lines of geochronological evidence suggest that the source material of the NWA7034 regolith breccia experienced a

thermal event around 1.7 to 1.4 Ga, with temperature estimates in the range of 500° to 800°C, as derived from a combination of isotopic and petrological observations (*31*). However, temperatures on the upper end of this range are only possible if short lived, and many authors favor a long-lived, low-temperature thermal event (*17*, *31*–*33*). Thermally activated diffusion to concentrate Y and rare earth elements into clusters throughout crystalline zircon requires temperatures of 800°C for 2 Ma (*27*). This is incompatible with any proposed thermal history now suggested for the source of the NWA7034 regolith breccia, making long-duration thermal diffusion an unlikely explanation for the observed clustering. Given the presence of {112} shock twins in the grain, the same impact event that created the shock twins likely also caused the nanoscale trace element clustering. Therefore, we suggest that the nanoscale trace element clustering and Fe enrichment along {112} twin planes occurred before the 1.7- to 1.4-Ga thermal episode, during a meteorite impact event as early as 4.3 Gyr (*10*) or 4.44 Gyr ago (*17*) that created the shock twins (Fig. 4). Prior studies have related the age of Pb clusters in terrestrial zircon to causative impact events (*28*, *30*). However, because of the overall low U concentration, the martian zircon analyzed here has insufficient radiogenic Pb to record the absolute timing of cluster formation, which remains speculative.

Implications for the early crust and hydrosphere of Mars

We propose that the 4.45-Ga crystallization age of the shocked zircon grain provides a minimum age for the presence of a magmatic hydrothermal system in the martian crust, under oxidizing conditions necessary to crystallize magnetic inclusions capable of recording the presence of a global geodynamo. The unusually high magnetism of the NWA7034 meteorite and paired stones compared to other martian meteorites and the compositional similarity of the polymict regolith breccia to the bulk composition of the martian crust have been cited to propose this rock as an analog for the strongly magnetized Noachian crust of Mars (*9*). This characterization is consistent with a proposed ejection site for these meteorites in the Terra Cimmeria-Sirenum province in the southern highlands of Mars (*34*). Terra Cimmeria-Sirenum is the most highly magnetic region of the martian crust and contains the Eridania basin, which preserves evidence of extensive hydrothermal alteration (*35*, *36*). Hydrothermal alteration has long been suggested as a possible cause for the highly magnetic properties of parts of the martian crust (*5*), a hypothesis supported by evidence for early (pre-Noachian or Noachian) hydrothermal activity preserved in the unusually water-rich and highly magnetic lithology of NWA7034 (*7*, *9*, *37*).

MATERIALS AND METHODS

Time-of-flight–secondary ion mass spectrometry

ToF-SIMS was used for high–spatial resolution chemical mapping of the major and trace elements in the zircon. An IONTOF M6 located in the John de Laeter Centre at Curtin University was used for the ToF-SIMS analysis. A 30-keV Bi^+ primary ion source was operated in Fast Imaging mode to achieve a lateral resolution of ~100 nm. The pulsed ion current was 0.15 pA. The ToF mass analyzer was operated in High Data Rate mode, and positive ions were collected up to a mass-to-charge ratio of ~310. The analyzed region was defined within a 50 μm–by–50 μm scan area to only include the grain of interest. The grain was pre-sputtered with an O_2

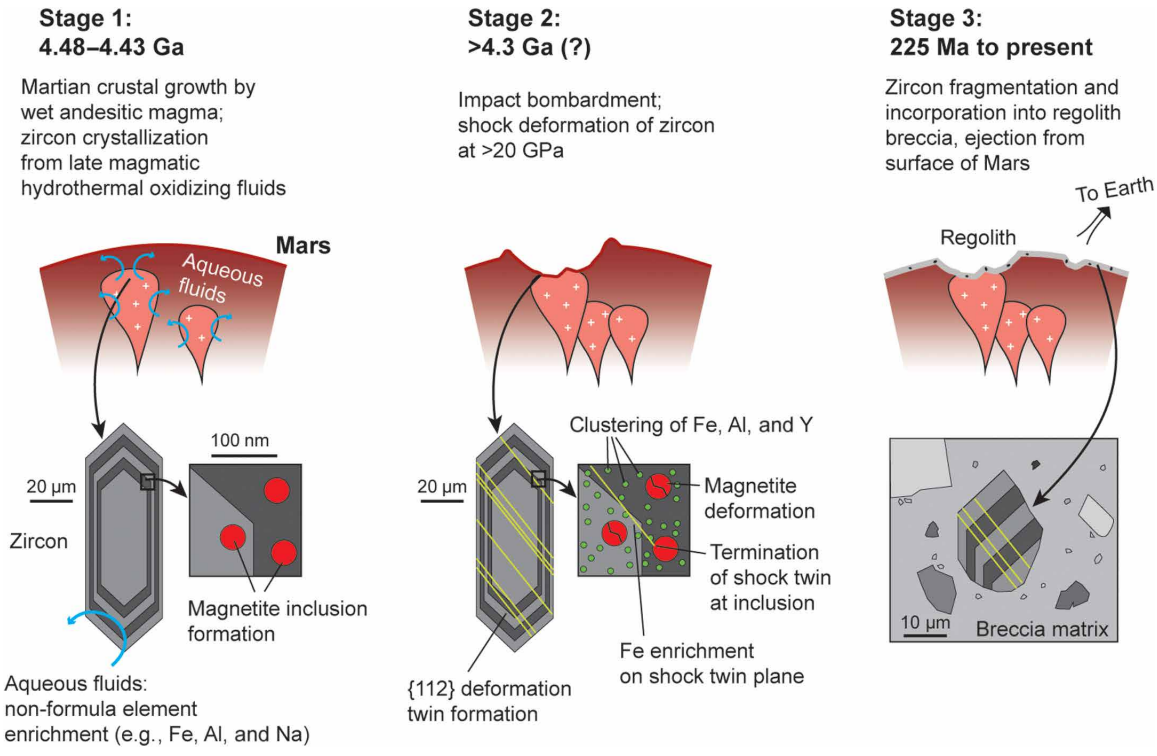

Fig. 4. Model of zircon growth and deformation in the context of the martian crust from 4.5 Ga to ejection of NWA7034 from Mars. Geological reconstruction based on the integration of results from prior work (*10*, *16*, *33*) and from this study.

ion source (1 kV, 235 nA) for 30 s to remove surface contamination. Data was analyzed using IONTOF Surface Lab version 7.3.

Transmission electron microscopy

Nanoscale study, HAADF STEM imaging, and EDS spot analysis/mapping were performed using an ultrahigh-resolution, probe-corrected, FEI Titan Themis S/TEM operated at 200 kV housed at Adelaide Microscopy at the University of Adelaide (*20*). This instrument is equipped with the X-FEG Schottky source and Super-X EDS geometry. The Super-X EDS detector provides geometrically symmetric EDS detection with an effective solid angle of 0.8 sr. Probe correction delivered sub-angstrom spatial resolution, and an inner collection angle greater than 50 mrad was used for HAADF experiments using the Fischione HAADF detector.

Atom probe tomography

APT has the capability of determining the distribution of major and trace elements at sub-nanometer resolution for mineral samples (*38*). The APT needle-shaped specimens were prepared using a Tescan Lyra3 Ga^+ focused ion beam coupled with a scanning electron microscope (FIB-SEM) at Curtin University. The position of the APT specimens was precisely targeted using electron beam deposited Pt fiducials (*39*). The specimens were analyzed using a Cameca LEAP 4000X HR at Curtin University. The instrument was operated in laser-assisted mode, using a ultraviolet ($\lambda = 355$ nm) laser. The laser was pulsed at 200-kHz repetition rate and a laser pulse energy of 300 pJ. During analysis, the specimens were kept at a base temperature of 60 K, and an automatic detection rate was set at 0.01 ions per pulse. In the mass-to-charge spectra, peaks twice higher than the background were ranged and identified for three-dimensional reconstruction using Cameca's AP Suite 6.3. Voltage evolution reconstructions were performed using a detector efficiency of 0.36, an image compression factor of 1.65, and a *k*-factor of 3.3. For reconstruction of zircon, an atomic volume of 0.01076 nm^3 per atom was used, and the electric field was empirically determined at 32 V/nm (*40*). The mass resolving power ($m/\Delta m$, where the peak width Δm is the full peak width at half its maximum height) of zircon APT data is ~1000, which provides good separation of peaks with differing mass numbers while not fully resolving isobaric interferences. However, there are no significant overlaps of the Fe, Al, and Y ion peaks with those of formula elements in zircon. Furthermore, the overlap between $^{27}Al^+$ and $^{54}Fe^{++}$ is easily de-convolved using the natural abundance of Fe isotopes among the Fe^{++} peaks, and the majority of Al is detected as Al^{++} at 13.5 Da, with no overlap with other ions. Trace element clusters were defined and analyzed using the maximum separation method (*41*), integrated into AP Suite 6.3, with $d_{max} = 2$ nm, $N_{min} = 15$, identifying a total of 320 clusters. Background correction was not required in the cluster analysis as the interference with background counts is expected to be insignificant when examining such spatially localized features.

Supplementary Materials

This PDF file includes:

Tables S1 and S2

REFERENCES AND NOTES

1. M. J. Van Kranendonk, R. Baumgartner, S. Cady, K. Campbell, B. Damer, D. Deamer, T. Djokic, A. Gangidine, S. Ruff, M. R. Walter, Terrestrial hydrothermal fields and the search for life in the solar system. *Bull. AAS* **53**, 10.3847/25c2cfeb.a3a646ab (2021).
2. B. M. Jakosky, R. J. Phillips, Mars' volatile and climate history. *Nature* **412**, 237–244 (2001).
3. J. F. Mustard, S. L. Murchie, S. Pelkey, B. Ehlmann, R. Milliken, J. A. Grant, J.-P. Bibring, F. Poulet, J. Bishop, E. N. Dobrea, Hydrated silicate minerals on Mars observed by the Mars Reconnaissance Orbiter CRISM instrument. *Nature* **454**, 305–309 (2008).
4. F. Poulet, J.-P. Bibring, J. Mustard, A. Gendrin, N. Mangold, Y. Langevin, R. Arvidson, B. Gondet, C. Gomez, Phyllosilicates on Mars and implications for early martian climate. *Nature* **438**, 623–627 (2005).
5. E. R. D. Scott, M. Fuller, A possible source for the Martian crustal magnetic field. *Earth Planet. Sci. Lett.* **220**, 83–90 (2004).
6. A. Goodwin, R. J. Garwood, R. Tartèse, A review of the "Black Beauty" martian regolith breccia and Its martian habitability record. *Astrobiology* **22**, 755–767 (2022).
7. C. B. Agee, N. V. Wilson, F. M. McCubbin, K. Ziegler, V. J. Polyak, Z. D. Sharp, Y. Asmerom, M. H. Nunn, R. Shaheen, M. H. Thiemens, A. Steele, M. L. Fogel, R. Bowden, M. Glamoclija, Z. Zhang, S. M. Elardo, Unique meteorite from early Amazonian Mars: Water-rich basaltic breccia Northwest Africa 7034. *Science* **339**, 780–785 (2013).
8. L. E. Nyquist, C.-Y. Shih, F. M. McCubbin, A. R. Santos, C. K. Shearer, Z. X. Peng, P. V. Burger, C. B. Agee, Rb-Sr and Sm-Nd isotopic and REE studies of igneous components in the bulk matrix domain of Martian breccia Northwest Africa 7034. *Meteorit. Planet. Sci.* **51**, 483–498 (2016).
9. J. Gattacceca, P. Rochette, R. B. Scorzelli, P. Munayco, C. Agee, Y. Quesnel, C. Cournède, J. Geissman, Martian meteorites and Martian magnetic anomalies: A new perspective from NWA 7034. *Geophys. Res. Lett.* **41**, 4859–4864 (2014).
10. M. A. Cox, A. J. Cavosie, K. J. Orr, L. Daly, L. Martin, A. Lagain, G. K. Benedix, P. A. Bland, Impact and habitability scenarios for early Mars revisited based on a 4.45-Ga shocked zircon in regolith breccia. *Sci. Adv.* **8**, eabl7497 (2022).
11. D. E. Moser, G. A. Arcuri, D. A. Reinhard, L. F. White, J. R. Darling, I. R. Barker, D. J. Larson, A. J. Irving, F. M. McCubbin, K. T. Tait, J. Roszjar, A. Wittmann, C. Davis, Decline of giant impacts on Mars by 4.48 billion years ago and an early opportunity for habitability. *Nat. Geosci.* **12**, 522–527 (2019).
12. D. E. Moser, C. L. Cupelli, I. R. Barker, R. M. Flowers, J. R. Bowman, J. Wooden, J. R. Hart, New zircon shock phenomena and their use for dating and reconstruction of large impact structures revealed by electron nanobeam (EBSD, CL, EDS) and isotopic U–Pb and (U–Th)/He analysis of the Vredefort dome. *Can. J. Earth Sci.* **48**, 117–139 (2011).
13. N. E. Timms, T. M. Erickson, M. A. Pearce, A. J. Cavosie, M. Schmieder, E. Tohver, S. M. Reddy, M. R. Zanetti, A. A. Nemchin, A. Wittmann, A pressure-temperature phase diagram for zircon at extreme conditions. *Earth Sci. Rev.* **165**, 185–202 (2017).
14. A. Wittmann, R. L. Korotev, B. L. Jolliff, A. J. Irving, D. E. Moser, I. Barker, D. Rumble III, Petrography and composition of Martian regolith breccia meteorite Northwest Africa 7475. *Meteorit. Planet. Sci.* **50**, 326–352 (2015).
15. H. Leroux, D. Jacob, M. Marinova, R. H. Hewins, B. Zanda, S. Pont, J.-P. Lorand, M. Humayun, Exsolution and shock microstructures of igneous pyroxene clasts in the Northwest Africa 7533 Martian meteorite. *Meteorit. Planet. Sci.* **51**, 932–945 (2016).
16. L. C. Bouvier, M. M. Costa, J. N. Connelly, N. K. Jensen, D. Wielandt, M. Storey, A. A. Nemchin, M. J. Whitehouse, J. F. Snape, J. J. Bellucci, F. Moynier, A. Agranier, B. Gueguen, M. Schönbächler, M. Bizzarro, Evidence for extremely rapid magma ocean crystallization and crust formation on Mars. *Nature* **558**, 586–589 (2018).
17. M. M. Costa, N. K. Jensen, L. C. Bouvier, J. N. Connelly, T. Mikouchi, M. S. Horstwood, J.-P. Suuronen, F. Moynier, Z. Deng, A. Agranier, The internal structure and geodynamics of Mars inferred from a 4.2-Gyr zircon record. *Proc. Natl. Acad. Sci. U.S.A.* **117**, 30973–30979 (2020).
18. P. W. O. Hoskin, U. Schaltegger, The composition of Zircon and igneous and metamorphic Petrogenesis. *Rev. Mineral. Geochem.* **53**, 27–62 (2003).
19. T. Geisler, U. Schaltegger, F. Tomaschek, Re-equilibration of Zircon in aqueous fluids and melts. *Elements* **3**, 43–50 (2007).
20. L. Courtney-Davies, C. L. Ciobanu, M. R. Verdugo-Ihl, A. Slattery, N. J. Cook, M. Dmitrijeva, W. Keyser, B. P. Wade, U. I. Domnick, K. Ehrig, J. Xu, A. Kontonikas-Charos, Zircon at the nanoscale records metasomatic processes leading to large magmatic–hydrothermal ore systems. *Minerals* **9**, 364 (2019).
21. J. A. Tarduno, R. D. Cottrell, W. J. Davis, F. Nimmo, R. K. Bono, A Hadean to Paleoarchean geodynamo recorded by single zircon crystals. *Science* **349**, 521–524 (2015).
22. B. P. Weiss, R. R. Fu, J. F. Einsle, D. R. Glenn, P. Kehayias, E. A. Bell, J. Gelb, J. F. D. F. Araujo, E. A. Lima, C. S. Borlina, P. Boehnke, D. N. Johnstone, T. M. Harrison, R. J. Harrison, R. L. Walsworth, Secondary magnetic inclusions in detrital zircons from the Jack Hills, Western Australia, and implications for the origin of the geodynamo. *Geology* **46**, 427–430 (2018).
23. F. Tang, J. M. Taylor Richard, F. Einsle Josh, S. Borlina Cauê, R. F. Roger, P. Weiss Benjamin, M. Williams Helen, W. Williams, L. Nagy, A. Midgley Paul, A. Lima Eduardo, A. Bell Elizabeth, T. M. Harrison, W. Alexander Ellen, J. Harrison Richard, Secondary magnetite in ancient zircon precludes analysis of a Hadean geodynamo. *Proc. Natl. Acad. Sci. U.S.A.* **116**, 407–412 (2019).
24. R. J. M. Taylor, S. M. Reddy, D. W. Saxey, W. D. A. Rickard, F. Tang, C. S. Borlina, R. R. Fu, B. P. Weiss, P. Bagot, H. M. Williams, R. J. Harrison, Direct age constraints on the magnetism of Jack Hills zircon. *Sci. Adv.* **9**, eadd1511 (2023).

25. E. A. Bell, P. Boehnke, T. M. Harrison, M. M. Wielicki, Mineral inclusion assemblage and detrital zircon provenance. *Chem. Geol.* **477**, 151–160 (2018).
26. L. Nasdala, P. W. Reiners, J. I. Garver, A. K. Kennedy, R. A. Stern, E. Balan, R. Wirth, Incomplete retention of radiation damage in zircon from Sri Lanka. *Am. Mineral.* **89**, 219–231 (2004).
27. J. W. Valley, A. J. Cavosie, T. Ushikubo, D. A. Reinhard, D. F. Lawrence, D. J. Larson, P. H. Clifton, T. F. Kelly, S. A. Wilde, D. E. Moser, M. J. Spicuzza, Hadean age for a post-magma-ocean zircon confirmed by atom-probe tomography. *Nat. Geosci.* **7**, 219–223 (2014).
28. T. B. Blum, D. A. Reinhard, M. A. Coble, M. J. Spicuzza, Y. Chen, A. J. Cavosie, L. Nasdala, C. C. N, T. J. Prosa, D. J. Larson, J. W. Valley, A nanoscale record of impact-induced Pb mobility in lunar zircon. *Microsc. Microanal.* **25**, 2448–2449 (2019).
29. E. M. Peterman, S. M. Reddy, D. W. Saxey, D. Fougerouse, D. R. Snoeyenbos, W. D. A. Rickard, Nanoscale processes of trace element mobility in metamorphosed zircon. *Contr. Mineral. Petrol.* **174**, 92 (2019).
30. G. A. Arcuri, D. E. Moser, D. A. Reinhard, B. Langelier, D. J. Larson, Impact-triggered nanoscale Pb clustering and Pb loss domains in Archean zircon. *Contr. Mineral. Petrol.* **175**, 59 (2020).
31. F. M. McCubbin, J. W. Boyce, T. Novák-Szabó, A. R. Santos, R. Tartèse, N. Muttik, G. Domokos, J. Vazquez, L. P. Keller, D. E. Moser, D. J. Jerolmack, C. K. Shearer, A. Steele, S. M. Elardo, Z. Rahman, M. Anand, T. Delhaye, C. B. Agee, Geologic history of Martian regolith breccia Northwest Africa 7034: Evidence for hydrothermal activity and lithologic diversity in the Martian crust. *J. Geophys. Res. Planets* **121**, 2120–2149 (2016).
32. J. J. Bellucci, A. A. Nemchin, M. J. Whitehouse, M. Humayun, R. Hewins, B. Zanda, Pb-isotopic evidence for an early, enriched crust on Mars. *Earth Planet. Sci. Lett.* **410**, 34–41 (2015).
33. W. S. Cassata, B. E. Cohen, D. F. Mark, R. Trappitsch, C. A. Crow, J. Wimpenny, M. R. Lee, C. L. Smith, Chronology of martian breccia NWA 7034 and the formation of the martian crustal dichotomy. *Sci. Adv.* **4**, eaap8306 (2018).
34. A. Lagain, S. Bouley, B. Zanda, K. Miljković, A. Rajšić, D. Baratoux, V. Payré, L. S. Doucet, N. E. Timms, R. Hewins, G. K. Benedix, V. Malarewic, K. Servis, P. A. Bland, Early crustal processes revealed by the ejection site of the oldest martian meteorite. *Nat. Commun.* **13**, 3782 (2022).
35. J. R. Michalski, E. Z. N. Dobrea, P. B. Niles, J. Cuadros, Ancient hydrothermal seafloor deposits in Eridania basin on Mars. *Nat. Commun.* **8**, 15978 (2017).
36. L. Ojha, S. Karunatillake, S. Karimi, J. Buffo, Amagmatic hydrothermal systems on Mars from radiogenic heat. *Nat. Commun.* **12**, 1754 (2021).
37. A. A. Nemchin, M. Humayun, M. J. Whitehouse, R. H. Hewins, J. P. Lorand, A. Kennedy, M. Grange, B. Zanda, C. Fieni, D. Deldicque, Record of the ancient martian hydrosphere and atmosphere preserved in zircon from a martian meteorite. *Nat. Geosci.* **7**, 638–642 (2014).
38. S. M. Reddy, D. W. Saxey, W. D. A. Rickard, D. Fougerouse, S. D. Montalvo, R. Verberne, A. van Riessen, Atom probe tomography: Development and application to the geosciences. *Geostand. Geoanal. Res.* **44**, 5–50 (2020).
39. W. D. A. Rickard, S. M. Reddy, D. W. Saxey, D. Fougerouse, N. E. Timms, L. Daly, E. Peterman, A. J. Cavosie, F. Jourdan, Novel applications of FIB-SEM-Based ToF-SIMS in atom probe tomography workflows. *Microsc. Microanal.* **26**, 750–757 (2020).
40. D. Fougerouse, D. W. Saxey, W. D. A. Rickard, S. M. Reddy, R. Verberne, Standardizing spatial reconstruction parameters for the atom probe analysis of common minerals. *Microsc. Microanal.* **28**, 1221–1230 (2022).
41. L. T. Stephenson, M. P. Moody, P. V. Liddicoat, S. P. Ringer, New techniques for the analysis of fine-scaled clustering phenomena within atom probe tomography (APT) data. *Microsc. Microanal.* **13**, 448–463 (2007).

Acknowledgments: A. Slattery at Adelaide Microscopy is thanked for technical support in the operation of the FEI Titan Themis S/TEM. **Funding:** This work was supported by the Swiss National Science Foundation, Ambizione grant PZ00P2_216313 (J.G.); Australian Research Council, Discovery Project DP190103849 and Discovery Project DP210100336 (D.F. and G.K.B.); Australian Research Council, LIEF program LE190100053; and Space Science and Technology Centre, Curtin University. **Author contributions:** Conceptualization: J.G., A.J.C., and D.F. Methodology: D.F., C.L.C., and W.D.A.R. Investigation: J.G., D.F., C.L.C., W.D.A.R., and D.W.S. Visualization: J.G. Writing—original draft: J.G. and A.J.C. Writing—review and editing: J.G., A.J.C., D.F., and C.L.C. Funding acquisition: G.K.B. and P.A.B. **Competing interests:** The authors declare that they have no competing interests. **Data and materials availability:** All data needed to evaluate the conclusions in the paper are present in the paper and/or the Supplementary Materials.

Submitted 16 May 2024
Accepted 22 October 2024
Published 22 November 2024
10.1126/sciadv.adq3694